Carbohydrate Polymers 292 (2022) 119680

Contents lists available at ScienceDirect

Carbohydrate Polymers

journal homepage: www.elsevier.com/locate/carbpol

Designing synergistic crystallization inhibitors: Bile salt derivatives of cellulose with enhanced hydrophilicity

Diana C. Novo [a,b], Chengzhe Gao [d], Qingqing Qi [d], Laura I. Mosquera-Giraldo [d,1], Glenn A. Spiering [c], Robert B. Moore [b,c], Lynne S. Taylor [d], Kevin J. Edgar [a,c,*]

[a] Department of Sustainable Biomaterials, Virginia Tech, Blacksburg, VA 24061, United States
[b] Department of Chemistry, Virginia Tech, Blacksburg, VA 24061, United States
[c] Macromolecules Innovation Institute, Virginia Tech, Blacksburg, VA 24061, United States
[d] Department of Industrial and Physical Pharmacy, College of Pharmacy, West Lafayette, IN 47907, United States

ARTICLE INFO

Keywords:
Olefin cross-metathesis
Bile-salts
Cellulose
Amorphous solid dispersion
Enzalutamide
Chemoselectivity

ABSTRACT

Crystallization inhibitors in amorphous solid dispersions (ASD) enable metastable supersaturated drug solutions that persist for a physiologically relevant time. Olefin cross-metathesis (CM) has successfully provided multifunctional cellulose-based derivatives as candidate ASD matrix polymers. In proof of concept studies, we prepared hydrophobic bile salt/cellulose adducts by CM with naturally occurring bile salts. We hypothesized that increased hydrophilicity would enhance the ability of these conjugates to maximize bioactive supersaturation. Their selective preparation presents a significant synthetic challenge, given polysaccharide reactivity and polysaccharide and bile salt complexity. We prepared such derivatives using a more hydrophilic hydroxypropyl cellulose (HPC) backbone, employing a pent-4-enyl tether (Pen) for appending bile acids. We probed structure-property relationships by varying the nature and degree of substitution of the bile acid substituent (lithocholic or deoxycholic acid). These conjugates are indeed synergistic inhibitors, as demonstrated with the fast-crystallizing prostate cancer drug, enzalutamide. The lithocholic acid methyl ester derivative, AcrMLC-PenHHPCPen (0.64), increased induction time 68 fold vs. drug alone.

1. Introduction

Bile acids are complex, interfacially active, amphiphilic compounds. They promote the emulsification of fats and solubilize poorly aqueous-soluble drugs through micelle formation (Mukhopadhyay & Maitra, 2004). These properties inspire use of bile acids and derivatives in biomedical applications, including to solubilize hydrophobic drugs and aid permeation (Pavlović et al., 2018). Bile acids can enhance supersaturated systems by promoting liquid-liquid or glass-liquid phase separation (LLPS or GLPS), stabilizing the sub-micron diameter droplets of highly concentrated drug (Jackson, Kestur, Hussain, & Taylor, 2016; Trasi & Taylor, 2015). Recently, bile salts have been shown to inhibit crystallization of structurally diverse drugs (Chen, Mosquera-Giraldo, Ormes, Higgins, & Taylor, 2015; Li et al., 2016; Lu et al., 2017a; Lu et al., 2017b). Molecular dynamic simulations indicate that van der Waals and hydrogen bonding interactions strongly influence crystallization inhibition (Li et al., 2016), while the degree of aggregation was found to influence effectiveness in delaying crystallization, as monomeric bile salts presented superior inhibition properties (comparable to HPMCAS-MF) for telaprevir (Lu et al., 2017a). Poorly water soluble drugs currently pose challenges for oral therapy. ASDs are molecular dispersions of drug in polymeric matrices, from which the drug rapidly dissolves in the gastrointestinal (GI) tract to form a supersaturated solution. ASD polymers play multiple roles, including providing adequately high formulation glass transition temperature (T_g) even when challenged by high humidity or drugs which are plasticizers, to prevent drug aggregation and crystallization. The polymer also must dissolve in the aqueous GI milieu at a rate similar to that of the drug (Craig, 2002; Taylor & Zhang, 2016). Sufficient dissolved polymer thereby can associate with the drug and prevent it from nucleating from the supersaturated solution, or if crystal seeds are present, from undergoing crystal growth via polymer adsorption to kinks or steps, therefore blocking molecular incorporation (Hasegawa et al., 1988). Some critical ASD challenges are still unmet by current polymers,

* Corresponding author at: Department of Sustainable Biomaterials, Virginia Tech, Blacksburg, VA 24061, United States.
E-mail address: kjedgar@vt.edu (K.J. Edgar).
[1] Current address: Pharmaceutical Candidate Optimization, Bristol Myers Squibb, Route 206 and Province Line Road, Princeton, NJ 08540, United States.

https://doi.org/10.1016/j.carbpol.2022.119680
Received 19 February 2022; Received in revised form 10 May 2022; Accepted 28 May 2022
Available online 31 May 2022

including formulations that must contain a high bioactive concentration, and/or where the drug is a fast crystallizer (Baird, Van Eerdenbrugh, & Taylor, 2010; Van Eerdenbrugh, Baird, & Taylor, 2010; Van Eerdenbrugh, Raina, Hsieh, Augustijns, & Taylor, 2014). Thus synthesis of high-performance ASD polymers is crucial, informed by elucidation of the complex and interwoven structure-property relationships that are key to meeting all performance criteria (Arca, Mosquera-Giraldo, Bi, et al., 2018; Frank & Matzger, 2018; Liu et al., 2014; Liu, Taylor, & Edgar, 2015; Mosquera-Giraldo et al., 2016; Mosquera-Giraldo, Borca, et al., 2018; Pereira et al., 2013; Ricarte et al., 2019; Wilson et al., 2020).

Recently we reported synthesis of the first model bile salts and steroids substituted with Grubbs type II olefins (Chatterjee, Choi, Sanders, & Grubbs, 2003; Dong, Matson, et al., 2017) as substrates for conjugation with cellulose ether derivatives, e.g. ethyl 5-pent-1-enyl cellulose (EC2.30C5) (Dong, Novo, Mosquera-Giraldo, Taylor, & Edgar, 2019a). The objective was to form a construct between these two known classes of crystallization inhibitors that would exhibit synergistic performance. While the CM approach was successful, these bile ester derivatives of polysaccharides did not exhibit the expected synergy. In fact they *reduced* the time to crystallization of the poorly soluble drug, telaprevir, vs. drug alone. We hypothesize that the hydrophobicity of both the ethyl cellulose backbone, (DS(Et) = 2.3, DS(Pen) = 0.7), and the bile acids caused the observed poor ASD performance, creating a mismatch between polymer and drug dissolution rates. We now hypothesize that bile salt/cellulosic polymer conjugates based on benign, water-soluble cellulose derivatives will have improved dissolution rates, therefore showing crystallization inhibition synergy.

We report attempts to design and prepare a series of conjugates with enhanced hydrophilicity, based on water-soluble HPC. Building on our previous work (Dong et al., 2019a), we sought to etherify HPC with a Type I olefin-terminated side chain for olefin CM (PenHPC) (Dong, Mosquera-Giraldo, Taylor, & Edgar, 2016). We broadened the series of bile acid derivatives by probing two attachment sites (A-ring OH vs. D-ring COOH) to determine which bile salt most influences crystal growth inhibition. Bile salt carboxyl groups were previously protected as methyl esters (Dong, Novo, Mosquera-Giraldo, Taylor, & Edgar, 2019b), while in this study we examine both ester and carboxylate-terminated conjugates. Carboxyl substituents are frequently elements of effective ASD polymers (Liu et al., 2014; Mosquera-Giraldo et al., 2016; Mosquera-Giraldo, Borca, et al., 2018). We investigate the influence of these polymers upon nucleation induction times of enzalutamide, an important, fast-crystallizing, hydrophobic drug for prostate cancer.

2. Experimental

2.1. Materials and methods

Hydroxypropyl cellulose (HPC, M_w = 100 kg mol^{-1}, DP = 100, DS (HP) 2.2, MS(HP) 4.4) (Dong, Mosquera-Giraldo, Troutman, et al., 2016)), sodium hydride (95%), anhydrous tetrahydrofuran (THF), 5-bromo-pent-1-ene, Hoveyda-Grubbs' 2nd generation catalyst, 3,5-di-*tert*-butylhydroxytoluene (BHT), triethylamine (TEA), lithocholic acid, deoxycholic acid, ethylene glycol, *para*-toluenesulfonyl hydrazide (*p*TSH), and potassium bromide (KBr) were from Sigma-Aldrich (Saint Louis, MO, USA). *N*,*N*-Dimethylacetamide (DMAc), *N*,*N*-dimethylformamide (DMF), lithium chloride (LiCl), dichloromethane (DCM), methanol, ethanol, and dialysis tubing (MWCO 3.5 k Da) were from Fisher Scientific (Fair Lawn, NJ, USA). Enzalutamide was obtained from ChemShuttle (Hayward, California).

^{1}H and ^{13}C NMR spectra were acquired on a Bruker Avance II spectrometer operating at 500 MHz except as indicated. Polymer (ca. 10 mg for ^{1}H NMR, 50 mg for ^{13}C NMR) was dissolved in ca. 1 mL $CDCl_3$ or dimethylsulfoxide (DMSO-d_6); CF_3CO_2H (three drops) was added to shift the water peak downfield. Fourier transform-infrared (FT-IR) spectra were recorded in transmission mode with a Thermo Nicolet 8700 instrument (Madison, WI, USA); samples prepared as KBr pellets (1 mg polymer/99 mg KBr mixed by mortar and pestle). Glass transition temperatures (T_g) were measured by a TA Instruments Q2000 using modulated differential scanning calorimetry (MDSC), with N_2 as purge gas. Each polymer sample (~0.3–6 mg in a Tzero aluminum pan) was first equilibrated at −50 °C and then heated as high as 270 °C at ramp rate 3 °C/min, with modulation amplitude of 1 °C and oscillation period of 60 s (results from first heating cycle). Molecular weights (M_w) were measured by size exclusion chromatography (SEC) applying a Wyatt Technologies TRIOS II light scattering and Optilab T-REX refractive index (RI) detectors, using two Agilent Technologies PLgel 10 μm mixed-bed columns, DMAc/LiCl solvent, and a Shimadzu LC-20AD at 50 °C at a flow rate of 1 mL min^{-1}.

2.2. Synthetic methods

2.2.1. Synthesis of hydroxypropyl 1-pent-4-enyl cellulose (PenHPC DS 0.60 and 1.00)

PenHPC (DS = 0.6, 1) was prepared according to Mosquera-Giraldo et al. (2016) (NMR (Fig. 2a, 3a), FTIR (Fig. S1a–d, top) and DS calculations (Fig. S7) in ESI (S1.1).

2.2.2. Syntheses of lithocholic acid (LCA) and deoxycholic acid (DCA) methyl esters

Syntheses carried out as adapted from Dong et al. (2019b); characterization information in ESI (S1.2).

2.2.3. Acrylation of A-ring bile acids and their methyl esters (exemplary procedure for LCA provided)

LCA (0.500 g, 1.32 mmol) was dissolved in anhydrous THF (5 mL, 0 °C), and triethylamine (0.134 g, 1 eq), then acrylic anhydride (Acr_2O, 0.201 g, 1.2 eq) was added gradually. The solution was stirred at RT for 20 h, then concentrated under rotary evaporation. The crude lithocholate 3-*O*-acrylate (AcrLC) product thus obtained was recrystallized from water. The product was isolated by filtration, then dried under vacuum at 80 °C. Methyl lithocholate acrylate (AcrMLC) and methyl deoxycholate acrylate (MDCAc) were prepared according to Dong et al. (2019b) (NMR data in ESI).

2.2.3.1. Lithocholate acrylate (AcrLC). Yield: 0.37 g, 64.5%. ^{1}H NMR (selected signals, $CDCl_3$): 0.63 (s, CH_3), 0.91 (s, CH_3), 0.93 (s, CH_3), 4.80 (m, 1H, C3 CH_2=CHCOOC<u>H</u>), 5.78 (dd, COOCH=C<u>H</u>$_2$, *trans*), 6.06 (dd, COOC<u>H</u>=CH_2), and 6.36 (dd, COOCH=C<u>H</u>$_2$, *cis*). ^{13}C NMR δ 12.1, 18.2, 20.8, 23.3, 24.2, 26.3, 26.6, 27.0, 28.2, 30.75, 31.0, 32.2, 34.6, 35.0, 35.3, 35.8, 40.1, 40.4, 41.9, 42.7, 55.9, 56.5, 74.6 (C3 CH_2=CHCOO<u>C</u>H), 129.1 (COOCH=<u>C</u>H$_2$), 130.2 (COO<u>C</u>H=CH_2), 165.8 (CH_2 = CH<u>C</u>OO), and 180.3 (<u>C</u>=OOH).

Deoxycholate acrylate (AcrDC) was prepared similarly by dissolving DCA (3.714 g, 9.57 mmol) in 20 mL anhydrous DCM containing 1 eq trimethylamine and 1 eq Acr_2O for 12 h. The solution was then concentrated under rotary evaporation, then the material was recrystallized from acetone, and collected as a pellet via centrifugation (0.782 g, 18% DCA). The liquid filtrate was collected, concentrated, and dried under vacuum at 80 °C. The resulting crude oil was then redissolved in DCM, and purified by column chromatography (silica gel, 15% EtOAc in DCM) to isolate the A-ring 3-*O*-acrylate, AcrDC (15% EtOAc/DCM, TLC Rf = 0.35), DCA (15% EtOAc/DCM, TLC Rf = 0), and *D*-ring 12-*O*-acrylate (15% EtOAc/DCM, TLC Rf = 0.65).

2.2.3.2. Deoxycholate acrylate (C3-O-AcrDC). Yield: 1.17 g, 27%. ^{1}H NMR (selected signals, $CDCl_3$): δ 0.69, 0.93, 4.00 (t, 1H, C12 HOC<u>H</u>), 4.80 (m, 1H, C3 CH_2=CHCOOC<u>H</u>), 5.78, 6.05, and 6.35. ^{13}C NMR (DMSO) δ 12.87, 17.41, 23.25, 23.72, 26.13, 26.61, 27.07, 27.56, 28.80, 30.78, 31.13, 32.26, 33.78, 34.27, 34.98, 35.18, 36.09, 41.97, 46.60, 47.43, 48.39, 73.36 (C3 CH_2=CHCOO<u>C</u>H), 74.58 (C12 HO-<u>C</u>H), 129.19 (COOCH=<u>C</u>H$_2$), 130.42 (COO<u>C</u>H=CH_2), 165.98 (<u>C</u>OOCH=CH_2), and

179.98 (24C C═OOH).

2.2.3.3. Deoxycholate diacrylate (C3 & C12-O-AcrDC). Yield: 2 g, 46.1%. ^{1}H NMR ($CDCl_3$) δ 0.86, 0.90, 0.92, 1.25, 1.48, 1.51, 1.62, 1.63, 1.69, 1.71, 1.80, 1.85, 2.24, 2.27, 2.33, 2.35, 2.37, 4.77, 5.17, 5.77, 5.80, 5.85, 5.88, 6.06, 6.08, 6.12, 6.16, 6.18, 6.20, 6.23, 6.34, 6.39, 6.42, and 6.46. ^{13}C NMR δ 12.45, 14.14, 17.40, 22.70, 23.09, 23.45, 24.69, 25.69, 25.91, 26.50, 26.88, 27.34, 29.07, 29.25, 29.37, 29.44, 29.60, 29.65, 29.67, 29.71, 30.56, 30.85, 31.93, 32.24, 33.97, 34.48, 34.66, 34.72, 35.69, 41.81, 45.23, 47.59, 49.64, 74.37, 76.00, 128.91, 129.03, 130.28, 130.61, 165.62, 179.60, and 179.88.

2.2.4. General procedure for olefin CM of PenHPC (DS (pen) =1.00)

Preparation of AcrLC-PenHPC(1.00) exemplifies the process: PenHPC(1.00) (190 mg, 0.22 mmol C═C), AcrLC (500 mg, 1.2 mmol, 2.9 equiv), and BHT (25 mg) were dissolved in ethyl acetate (EtOAc,12 mL) under N_2. HG II catalyst (39 mg, 12 mol%) was dissolved in anhydrous EtOAc (1 mL) and gradually added to the solution, which was stirred at 50 °C for 3 h before adding three drops of ethyl vinyl ether to terminate the reaction. The solution was concentrated under vacuum and added to hexanes to precipitate the product, which was redissolved in THF and reprecipitated into water, then dried overnight under vacuum at 40 °C. Additional NMR data in ESI, S1.3.

2.2.4.1. AcrLC-PenHPC(1.00). Yield: 350 mg, 87.5%. ^{1}H NMR ($CDCl_3$): δ = 0.64 (s, CH_3), 0.91 (s, CH_3), 0.92 (s, CH_3), 1.00–2.57 (m, steroid ring protons, OCH_2CH_2CH_2CH═CHCOO-LCAc), 2.90–4.68 (m, cellulose backbone, OCH_2CH_2CH_2CH═CHCOO-LCAc, 4.77 (m, LCAc C3 CH), 5.77 (OCH_2CH_2CH_2CH═CHCOO-LCAc), and 6.94 (OCH_2CH_2CH_2CH═CH-COO-LCAc). ^{13}C NMR (126 MHz, DMSO) δ 12.32, 17.78, 18.59, 20.71, 23.50, 24.28, 24.90, 25.71, 26.44, 26.76, 28.19, 28.89, 29.52, 29.81, 31.16, 32.38, 34.62, 35.27, 35.76, 41.64, 42.72, 56.05, 56.40, 65.73, 67.97, 68.52, 72.98–79.16 (cellulose C2, C3, C5 and bile acid C3 CH_2═CHCOOCH), 83.10 (cellulose C4), 101.72 (cellulose C1), 121.78 (OCH_2CH_2CH_2CH═CHCOO-LCAc), 149.38 (OCH_2CH_2CH_2CH═CHCOO-LCAc), 172.65 (C═OOAcrLC), and 175.25 (24C C═OOH).

2.2.5. General procedure for hydrogenation of PenHPC-bile ester conjugates

Preparation of AcrDC-PenHHPC(1.00) was adapted from Dong et al. (2019b); all details found in ESI (S1.4), with remaining hydrogenated product characterizations on (Fig. S4 and S6).

2.2.5.1. AcrDC-PenHHPC(1.00). Yield: 160 mg, 71%. ^{1}H NMR (selected, DMSO) δ 0.58 (s, CH_3) 0.86 (s, CH_3), 1.01–2.21 (m, steroid ring protons, OCH_2CH_2CH_2CH_2CH_2COO-DCAcAn), 2.76–4.54 (m, cellulose backbone, OCH_2CH_2CH_2CH_2CH_2COO-DCAcAn, C12 HO-CH), and 4.60 (DCAcAn C3 –OCH). ^{13}C NMR δ 12.44, 16.94, 17.34, 19.12, 20.29, 22.83, 23.49, 24.45, 25.25, 25.92, 26.14, 26.67, 27.18, 28.53, 29.37, 30.77, 30.88, 31.89, 32.83, 33.79, 34.55, 34.97, 35.55, 41.18, 46.03, 46.24, 47.42, 64.98, 65.29, 68.14, 71.06–79.28 (cellulose C2, C3, C5, and bile ester C3 CH_2CH_2COOCH and C12 HO-CH), 82.52 (cellulose C4), 101.37 (cellulose C1), 172.28 (C═OODCAc), and 174.97 (C═OODCAc).

2.2.6. Selective hydrolysis of D-ring methyl ester, AcrMLC-PenHHPC

AcrMLC-PenHHPC(1.00) (250 mg, 0.29 mmol –OMe) dissolved in 5 mL THF was heated to reflux (~59 °C) with stirring, followed by dropwise addition of 2 M NaOH (5 mL). The solution was stirred 1 h, then cooled to RT, followed by partitioning between EtOAc/water; water extraction was repeated 3×. Aqueous layer was dialyzed against methanol (1 day) and water (2 days), then lyophilized.

Yield: 18%, ^{1}H and ^{13}C NMR signals agreed with those of AcrLC-PenHHPC obtained via direct acrylation and CM of the bile acid (Section 2.2.5).

2.3. Measurement of nucleation induction times

Polymer was dissolved in DMSO (20 mg/mL) by sonication (60 min, 40 °C). Next, small aliquots (125 μL) of this solution were added, using constant agitation, to 50 mL of pH 6.8100 mM buffer at 37 °C to obtain 50 μg/mL polymer solutions (<1% DMSO). Supersaturated enzalutamide solutions (35 μg/mL) were prepared by adding 175 μL of the enzalutamide methanolic stock solution (10 mg/mL) to 50 mL phosphate buffer (0.100 M) with polymer concentration 50 μg/mL, maintained at 37 °C and magnetically stirred (300 rpm). Crystallization induction time from unseeded samples was measured using an SI Photonics UV/vis spectrometer (Tucson, AZ) coupled to a fiber optic probe (path length 5 mm). Wavelength scans (200–450 nm) were performed at 60 s time intervals. Crystal formation onset time was determined from the drop in drug concentration (absorbance at 237 nm) in the absence and presence of pre-dissolved polymer at 37 °C, designated as the nucleation induction time; measurement repeated 3×.

2.4. Solubility parameter (SP) calculation

Cellulose derivatives and enzalutamide SP were determined using Fedor's method (Fedors, 1974). Procedural details in ESI of Dong, Mosquera-Giraldo, Taylor, et al., 2016.

3. Results and discussion

Our strategy exploited the 4-pent-1-enyl ether of HPC (PenHPC, Scheme 1) as the Grubbs Type I olefin in CM (Dong, Mosquera-Giraldo, Troutman, et al., 2016; Grubbs, 2004) with an acrylated bile salt derivative (Type II olefin). We faced chemoselectivity challenges, including selectivity between the neutral A-ring hydroxyl and the anionic D-ring carboxylate nucleophiles of LCA.

The DCA A-ring OH-nucleophile competes with both the D-ring carboxylate and the C-ring hydroxyl. Cellulose derivatives are relatively unreactive since they diffuse slowly, have relatively high Mw, and hydroxyls have relatively narrow approach angles; all non-conducive to regioselectivity (Fox, Li, Xu, & Edgar, 2011). Fortunately, PenHPC has a flexible oligo(HP) tether and broader approach angles.

The key issue was selective bile salt acrylation. We began by making bile acid methyl esters to eliminate carboxylate/hydroxyl competition (Scheme 1). LCA (methyl lithocholate, MLC) and deoxycholic acid (methyl deoxycholate, MDC) esters were prepared by Fischer esterification (Fischer & Speier, 1895) as reported previously (Dong et al., 2019b). Acrylation of bile salt methyl esters was by Dong's procedures, catalyzed by triethylamine at 0 °C using Acr_2O, with excellent yield from MLC, and moderate, somewhat selective acrylation yield from difunctional MDC. ^{1}H NMR spectra for bile acid and acrylates are shown on Fig. 1; ^{13}C NMR spectra are in Fig. S2. As exemplified for LCA reactions, successful methyl esterification was confirmed by the new ^{1}H NMR singlet at 3.66 ppm and the methyl ester ^{13}C NMR resonance (C25) at 51.39 ppm. Subsequent A-ring hydroxyl acrylation was confirmed by downfield shift of the C3-OCH methine multiplet (3.62 to 4.66 ppm) due to presence of 3-*O*-acrylate (Fig. 1b). Product acrylate olefin protons were observed as doublets (5.79, 6.10, 6.39 ppm) (Fig. 1b), with corresponding ^{13}C NMR quaternary resonances (129.15, 130.2 ppm) (Fig. S2b).

Direct bile salt acrylation would afford a carboxyl-functionalized adduct, which we hypothesized would be an effective crystallization inhibitor based on earlier structure-property studies (Mosquera-Giraldo et al., 2016; Mosquera-Giraldo, Li, et al., 2018). We chose Acr_2O to effect selective acrylation of the less hindered LCA A-ring hydroxyl (Dong et al., 2019b; Hu, Zhang, Zhang, Li, & Zhu, 2005; Li & Ray Dias, 1997; Zhu & Nichifor, 2002; Table 1). C3-OH selectivity was maximized by limiting the Acr_2O/OH ratio. One equivalent each of Acr_2O and triethylamine worked best; after 20 h, we were gratified to observe complete C3-OH chemoselectivity. Purity and identity of the 3-*O*-acrylated

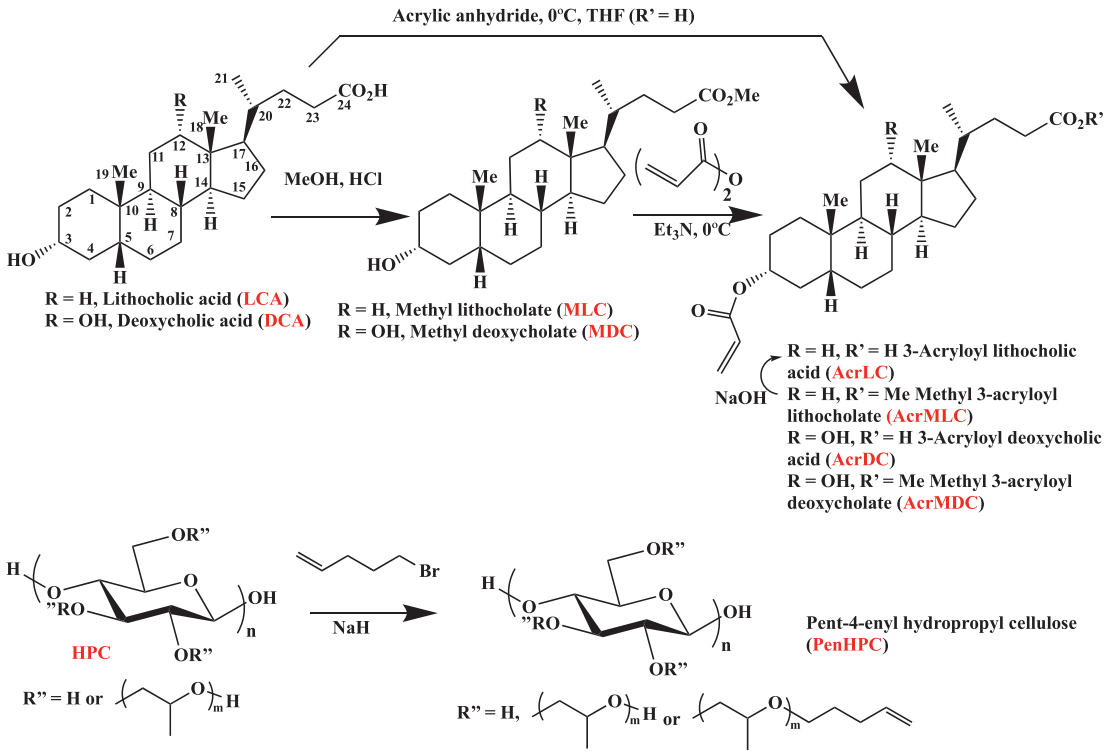

Scheme 1. CM partner syntheses. Structures do not imply regioselectivity; particular positions of substitution in all schemes only for convenience of depiction and clarity.

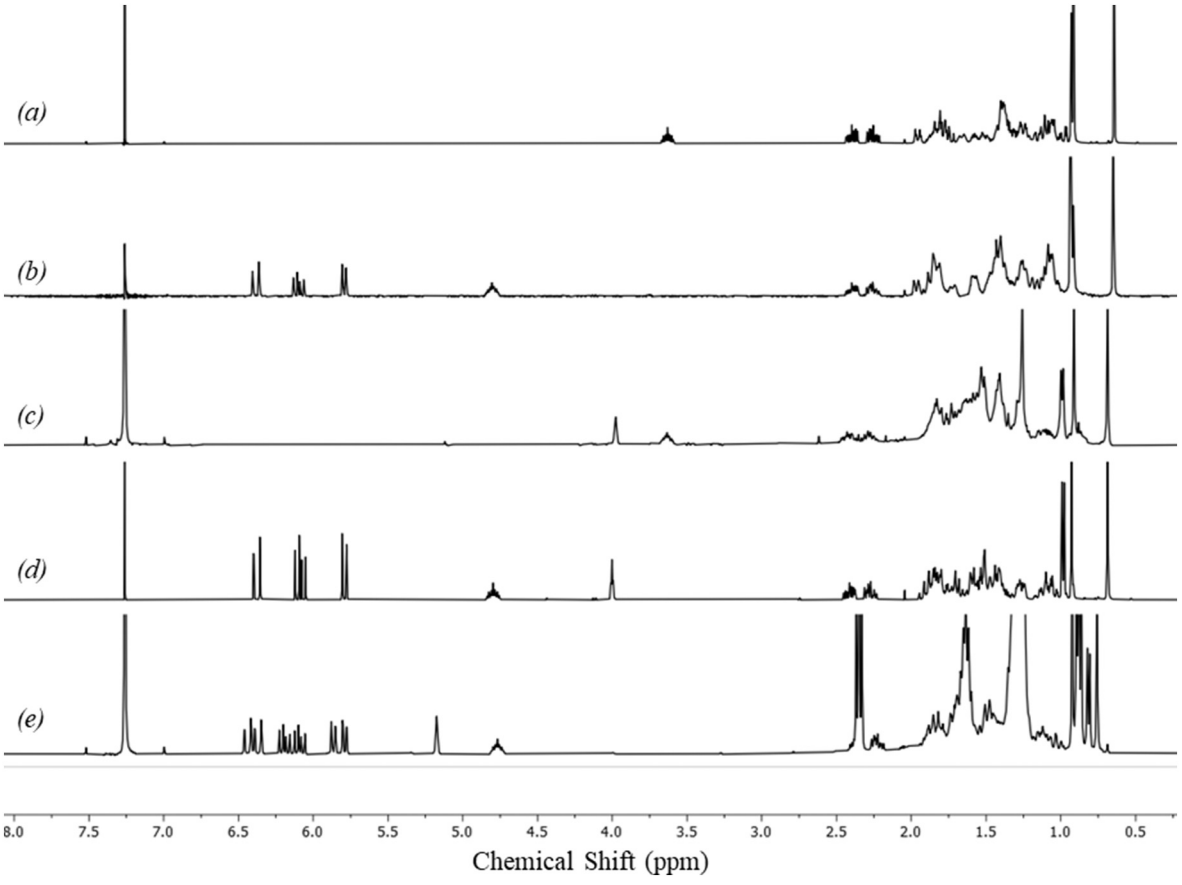

Fig. 1. Proton NMR spectra of a) LCA, b) acrylated LCA (AcrLC), c) DCA, d) monoacrylated C3-OAc DCA (AcrDC), and e) diacrylated DCA (AcrDC).

Table 1
Selectivity vs. conditions for esterification of A-ring hydroxyl (C3-OH).

Substrate	Acrylate/TEA molar ratio	Time (h)	Starting material (%)	3-*O*-Acrylate (%)	12-*O*-Acrylate (%)
LCA	1.2:1	12	0	100	n/a
		16			
		16			
	1.2:3	12	56.7	43.2	n/a
	1.2:5	12	31	69	n/a
DCA	1.2:1	12	42	57	20
		16	63	36	29
		16	40*	50*	30*
	1.2:3	16	60*	41*	32*

* 16 h using acryloyl chloride.

AcrLC product were confirmed by FTIR and NMR spectroscopy. Downfield shift of the 3-CH-OH proton (3.63 to 4.66 ppm) upon acrylation was diagnostic; (Fig. 2a, b), supported by the downfield ^{13}C NMR shift of C3-OAcr (71.39 to 74.6 ppm). Additional strong evidence was provided by the acrylate proton resonances (5.79, 6.05, 6.36 ppm), acrylate carbons (129.1, 130.2), and the new ester carbonyl (165.8 ppm) (Fig. 2b, Fig. S3c). FT-IR spectroscopy was also supportive, with new olefinic stretches at 1621 cm^{-1} (Fig. S1).

With its additional C-ring hydroxyl (C12-OH), regioselective DCA acrylation is more challenging (Hu et al., 2005). We sought selectivity by brief esterification with Acr_2O at 0 °C. Selectivity was modest, affording 57% 3-*O*-Ac, 20% 12-*O*-Ac, and 42% unreacted DCA by ^{1}H NMR (emergence of three acrylate olefin protons, and characteristic downfield shifts protons alpha to acrylation sites). Disappearance of the methine (alpha to methoxyl) resonance at 3.62 ppm was accompanied by emergence of the 3-*O*-Ac C3-OCH monoacrylate at 4.44 ppm, as well as new olefinic protons (5.78, 6.05, 6.35 ppm) (Fig. 1d); analogously, the C12-OCH methine proton (4.0 ppm) disappeared, replaced by the deshielded monoacrylate 12-*O*-Ac-OCH (5.17 ppm), whereas new olefinic acrylate protons emerged (5.84, 6.16, 6.40 ppm) in the diacrylate mixture (Fig. 1e). Longer reaction times, more acrylate, and use of more reactive acryloyl chloride all harmed regioselectivity (Table 1). Despite modest selectivity, we were able to isolate pure deoxycholic acid 3-acrylate by flash column chromatography.

Our previous successful CM with ethyl pent-4-enyl cellulose (EC2.30C5; Dong et al., 2019b) inspired the methodology herein, reacting PenHPC (Grubbs type I olefin) with acrylated bile acids and esters (Grubbs Type II olefins) (Chatterjee et al., 2003; Dong, Matson, et al., 2017). Exemplary reaction of 3-*O*-acryloyl-lithocholic acid (AcrLCA) with pent-4-enyl HPC is shown (Scheme 2).

We explored effects of solvent (EtOAc, THF, DCM) and temperature (37, 50 °C) on CM reaction time and conversion (Table 2). Earlier bile ester CM conjugation with ethyl cellulose derivatives reached completion within 24 h (37 °C) (Dong et al., 2019b), but here we made the useful observation that EtOAc accelerates CM, affording higher efficiency (<equiv. (2.9) of precious acrylate required, vs. 5 equiv. in THF or CH_2Cl_2 (Dong et al., 2019b)) in reaching 100% conjugation. Even with this smaller excess, kinetics in EtOAc were significantly faster; 100% conversion within 5 h at 37 °C. At 50 °C, achievable because of the higher EtOAc boiling point, 100% completion was reached within 3 h even at only 2.9:1 type II:type I olefin.

Conjugate formation was monitored by disappearance of terminal olefin proton resonances (4.96, 5.82 ppm) from PenHPC and 5.78–6.36 ppm from the acrylates (e.g. Fig. 2a, b) along with emergence of new, distinct conjugated olefin proton resonances (5.82, 6.89 ppm). Products also showed expected steroid nucleus proton resonances, between 2.4 and 0.6 ppm (Fig. 2c). Adduct structures were further supported by new olefinic carbon resonances (Figs. 3b, S3), which shifted as expected upon conjugation (PenHPC from 114.5, 138.4; acrylate from 129.1, 130.2

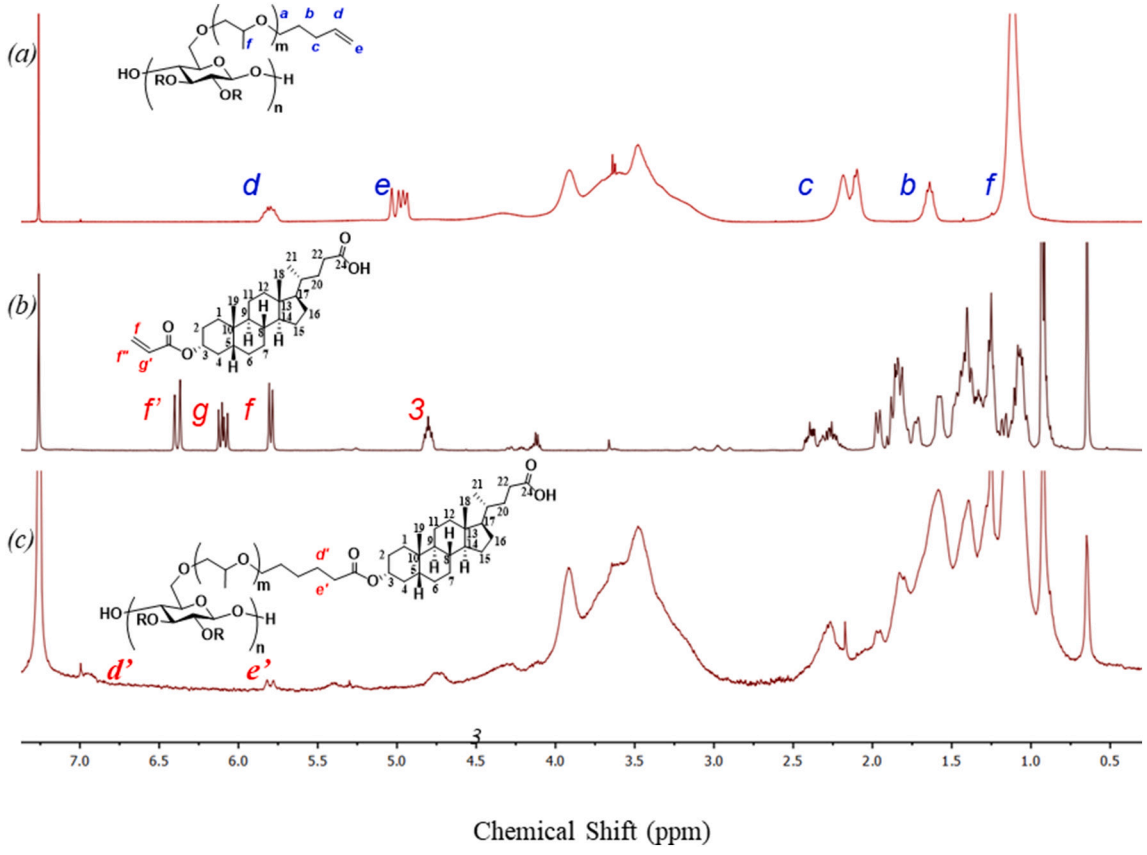

Fig. 2. Proton NMR spectra of a) PenHPC b) AcrLC, c) CM conjugate, 3-*O*-PenHHPC lithocholate (1.00).

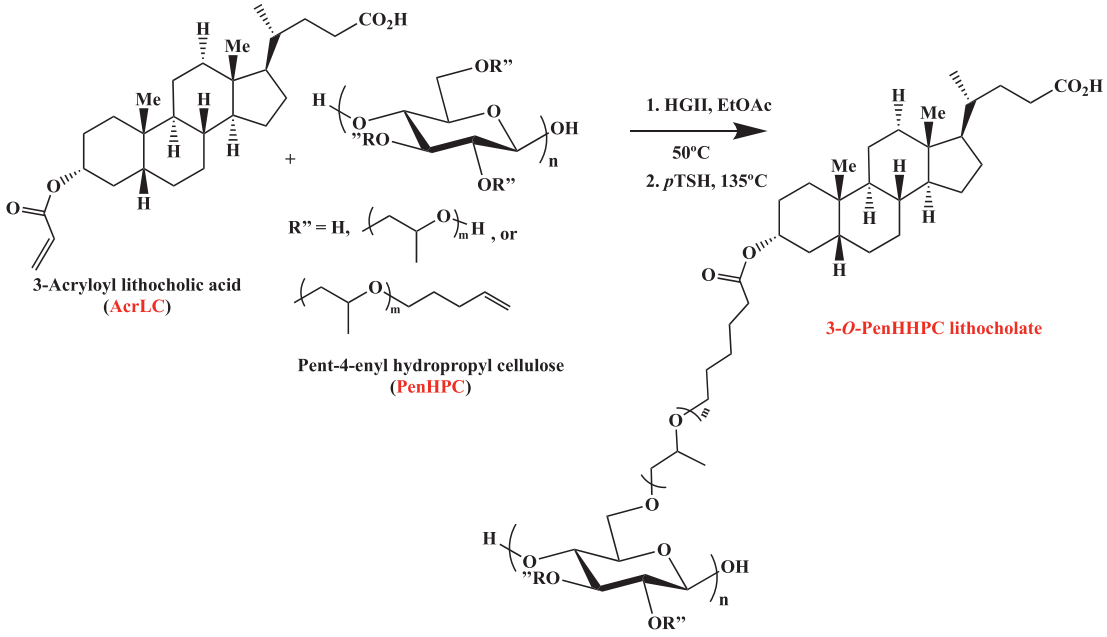

Scheme 2. Bile salt CM chemistry.

Table 2
Reaction times, conversion achieved ($DS_{bile\ acid\ conjugate}$) vs. acrylated bile acid, solvent, and reaction temperature.*

PenHPC DS (pent-4-enyl)	Solvent, (temp. (°C))	Conversion (reaction time, h)			
		AcrMLC	AcrLC	AcrMDC	AcrDC
1.00	THF (37 °C)	100 (36)	–	–	–
	DCM (37 °C)	100 (14.5)	50 (12)	–	–
	EtOAc (50 °C)	100 (3)	100 (3)	100 (3)	100 (3)
0.60	THF (37 °C)	50 (39.5)	50 (39.5)	–	–
	DCM (37 °C)	80 (24)	100 (54)	–	–
		100 (36)	–	–	–
	EtOAc (50 °C)	100 (3)	100 (3)	100 (3)	100 (3)

* Catalyst HGII, 10 mol%.

ppm) to 121 and 149.4 ppm, respectively (Fig. 3a, b). After CM completion, we demonstrated the possibility of recovering valuable, unreacted bile salt acrylate, by concentrating the hexanes filtrate after precipitation, and redissolving the resulting crude solid in minimal solvent for subsequent injection into a silica plug for further isolation from residual catalyst or polymer. The more polar PenHPC or PenHPC-bile ester conjugate residue was retained by the silica, while the less polar acrylate and potentially some HG II catalyst coeluted with the mobile hexanes, from which it was readily recovered by evaporation.

We have previously shown that α, β-unsaturated CM products are prone to radical-initiated γ-H-atom abstraction (Meng & Edgar, 2015), followed by undesired radical reactions. We eliminated this risk in our CM adducts by final transfer hydrogenation of the conjugated olefins (Dong & Edgar, 2015; Dong, Mosquera-Giraldo, et al., 2017; Meng & Edgar, 2015; Meng, Matson, & Edgar, 2014), refluxing the conjugate at 135 °C in the presence of *p*-toluene sulfonyl hydrazide (*p*TSH). Complete hydrogenation was clearly indicated by the absence of vinyl proton or carbon resonances in product ^{1}H and ^{13}C NMR spectra (Fig. S4). Further, expected FT-IR shifts and absorbance reductions were observed for conjugates and their corresponding hydrogenated products (Fig. S1a–d, bottom). We refer to the hydrogenated conjugate of PenHPC and AcrLC as 3-*O*-PenHHPC lithocholate (Scheme 2; where the "H" that precedes "HPC" refers to "hydrogenated"); in this case DS(pent-4-enyl) was 1.0 (exemplary ^{1}H NMR spectra Figs. 2, 3).

We demonstrated selective hydrolysis of 3-*O*-PenHHPC lithocholate D-ring methyl ester. Hydrolysis was performed after hydrogenation, via brief reflux (2 M NaOH, 1 h). This afforded a ready, straightforward approach to obtain two of our target compounds (methyl ester- or carboxylic acid-bearing), avoiding potential cleavage of acrylate ester. In spite of this success, purification afforded a modest yield (~18%). It is possible that, despite the brief heating, sufficient depolymerization may have occurred to cause polymer loss during dialysis (MWCO 3.5 kDa).

Polymers with sufficiently high T_g (40–50 °C above ambient temperature) are desired to combat effects of humidity and possible drug plasticization upon the formulation. Many cellulose derivatives have high T_g values (Dong et al., 2019a), but it was important to investigate possible internal plasticization by bile acid substituents. PenHPC (DS (Pen) = 1.00) T_g is 91 °C, (Dong, Mosquera-Giraldo, Taylor, et al., 2016). Each hydrogenated conjugate displayed T_g well above ambient temperature, from 80.71 to 145 °C, though some were quite weak. The higher *Tg* derivatives have significant potential for sustaining ASD formulations in the glassy state (Fig. S9–16, Table S1).

We tested performance of these complex bile acid- and bile ester-tethered polysaccharides in vitro as drug crystallization inhibitors. The time at which drug crystallization became detectable due to drop in drug solution content (inflection point in A_{237nm}) was designated as the nucleation induction time, measured in the absence and presence of each polymer. Enzalutamide is a hydrophobic, fast crystallizing, poorly water-soluble (crystalline solubility = 2.9 μg/mL) prostate cancer therapeutic (Wilson et al., 2018).

We had hypothesized that more hydrophilic polymers would result in effective crystallization inhibition. In the absence of polymer (Fig. 4), the drug crystallized quickly, within 7 min.

Previous studies showed the importance of carboxylic acids in effective crystallization inhibitors (Mosquera-Giraldo et al., 2016), but also showed that higher DS(CO_2H) at some point does not enhance polymer effectiveness (Mosquera-Giraldo, Borca, et al., 2018). Using computer simulations, we have shown that drug molecules tended to interact with the hydrophobic portion of the polymer rather than forming specific interactions with the carboxylic acids. This suggested that carboxylic acids may provide amphiphilicity, but do not necessarily

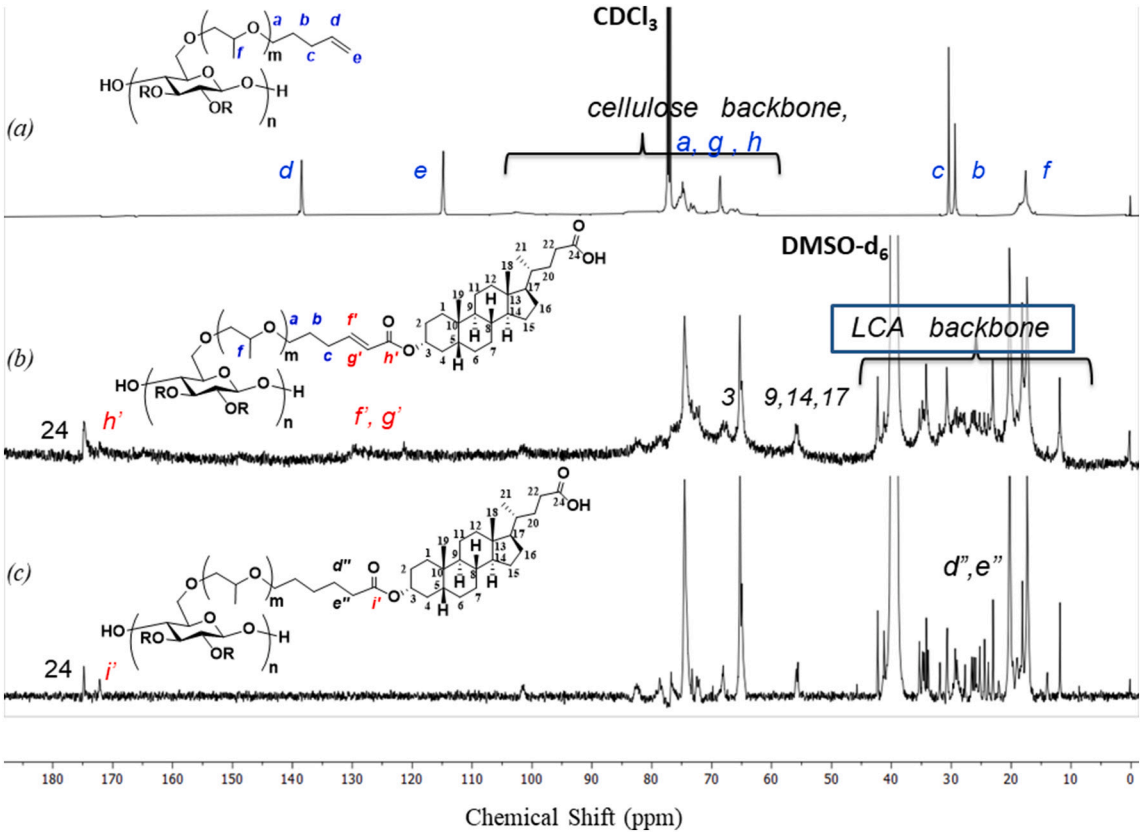

Fig. 3. ^{13}C NMR spectra of a) PenHPC b) AcrLC, c) CM conjugate, 3-*O*-PenHHPC lithocholate (1.00).

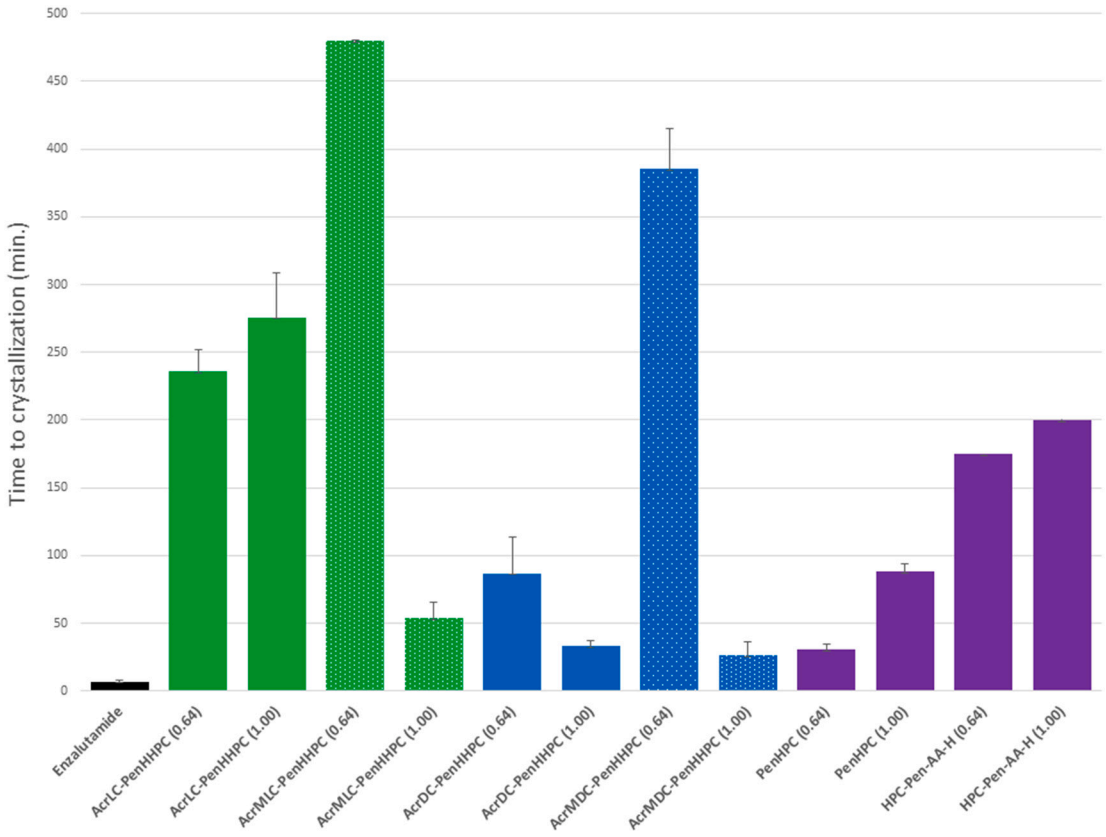

Fig. 4. Enzalutamide nucleation induction times in absence and presence of pre-dissolved polymers (n = 3; polymer abbreviations and structures see Table S2).

form specific interactions with drug molecules. Herein, we found that the best performing ASD polymers with regard to inhibition of enzalutamide crystallization were methyl esterified, in particular those with lower DS(bile salt ester). 3-*O*-PenHHPC methyl lithocholate (DS(bile ester) 0.64) can effectively maintain supersaturation for ca. 8 h (when experiment was terminated). Meanwhile, 3-*O*-PenHHPC methyl deoxycholate (DS bile ester 0.64) afforded induction time until crystallization of ca. 385 min. It appears that for enzalutamide, hydrophobic interactions between bile salt ester and drug were more important than amphiphilicity provided by the carboxylic acid substituents, which seemed to be of importance for many polysaccharide derivatives (Arca, Mosquera-Giraldo, Pereira, et al., 2018; Dong, Mosquera-Giraldo, et al., 2017; Dong, Mosquera-Giraldo, Troutman, et al., 2016; Ilevbare, Liu, Edgar, & Taylor, 2013b; Liu et al., 2014; Tanno, Nishiyama, Kokubo, & Obara, 2004). Alternatively, the combination of bile ester and hydrophilic cellulose ether backbone generates a degree of ampiphilicity that enables the appropriate balance between polymer-water interactions and polymer-drug interactions, as suggested in previous studies (Mosquera-Giraldo, Borca, et al., 2018). All of our bile acid/ester conjugates with HPC pentyl ether prolonged enzalutamide crystallization time. We were pleased to observe that LCA derivatives (simpler to make) consistently out-performed DCA derivatives.

We compared performance of these novel ASD polymer candidates to their cellulose ether precursors (pent-4-enyl HPC, DS(pent-4-enyl) 0.64, 1.0), which were not conjugated to bile salts and thus could serve as negative controls. As positive controls, we used CM adducts of pentenyl HPC with acrylic acid (after hydrogenation), HPC-Pen-AA-H (0.64) and HPC-Pen-AA-H (1.00), since we previously shown that they are effective crystallization inhibitors (Wilson et al., 2020). Enzalutamide crystallizes in <150 min using similar conditions (50 μg/mL polymer, 50 mM phosphate buffer) in the presence of 5-carboxypentyl HPC with DS (carboxypentyl) 1.0 (Wilson et al., 2020), supporting the concept that sufficiently hydrophilic bile salt-appended cellulose ethers are synergistic and effective crystallization inhibitors.

Fedor SPs of our derivatives were calculated (Table S3). Effective crystallization inhibitors have been associated with moderate hydrophobicity, ranging from SP 20–23 $MPa^{1/2}$ for promising cellulose esters (Ilevbare et al., 2013b; Ilevbare, Liu, Edgar, & Taylor, 2013a) and ethers (Dong, Mosquera-Giraldo, Taylor, et al., 2016). The pentenyl HPC derivatives are more hydrophilic, with SP values 22.8 and 21.8 $MPa^{1/2}$ for DS (Pen) = 0.64 and 1, respectively; vs. the more hydrophobic pentenyl substituted EC2.30C5 DS(Pen) = 0.69 (SP values 18.0 to 19.9 $MPa^{1/2}$). Thus SP values for HPC-bile salt adducts prepared herein, falling within 21.0–23.2 $MPa^{1/2}$ indicate improved hydrophilicity, which contributes to longer nucleation induction times in most cases.

4. Conclusions

We confirmed our original hypothesis by demonstrating synergistic, enhanced ASD performance of conjugates of bile acids with HPC derivatives, with their improved hydrophilicity. Grubbs Type II olefin acrylates of bile salts or their methyl esters were prepared chemo- and regioselectively by acrylation of bile salts and esters, followed by efficient, mild CM, in order to probe both A- and D-ring structure-property relationships regarding crystal growth inhibition. Careful selection of acrylating agent, minimizing its excess, and optimizing base stoichiometry allowed us to achieve chemoselective acrylation of the LCA A-ring hydroxyl. By so doing we eliminate the extra methyl esterification step as well as the sensitive saponification of the methyl ester in the presence of the acrylate ester. These methods also provided a degree of regioselectivity in acrylation of the equatorial 3-OH of DCA in the A-ring vs. to the C-ring 12-OH. We significantly improved both CM kinetics and efficiency of preparing these complex structures by optimizing conditions. EtOAc provides much faster CM conversion. Rates of initiation in olefin methathesis are known to increase with solvent polarity (Sanford, Love, & Grubbs, 2001), and DCM (20.2) has a higher Hildebrand SP than EtOAc (18.2), so the faster rates in EtOAc are an important and pleasant surprise. The higher EtOAc boiling point must certainly be influential on kinetics; for example, AcrMLC CM completion in EtOAc taking 3 h at 50 °C vs. 14.5 h in DCM at 37 °C (Table 2). Although their polarities are similar and THF boiling point is slightly higher (Hildebrand SP 18.3, BP 66 °C (Sanford et al., 2001)), CM was faster in EtOAc than in THF, 100% conversion of AcrMLC in the latter solvent for example taking 36 h. The better ability of THF to coordinate metals may be a factor, perhaps by competing for Ru coordination sites. Superior CM performance in EtOAc promises greater efficiency than previously reported bile salt CM chemistry (Dong et al., 2019a), reducing usage of expensive bile acid starting materials, and allowing recycle of unreacted bile salt acrylate; virtually 100% efficiency with regard to bile salt acrylate may be possible.

These results illuminate structure-property relationships of bile acid vs. bile ester decorated polysaccharides for oral drug delivery, simultaneously highlighting the remarkable potential of mild, flexible, and efficient CM chemistry for synthesis of complex polysaccharide derivatives. It is worth emphasizing that even with large, sterically demanding, slow diffusing molecules like these cellulose derivatives, and even when the CM type II olefin partner is a relatively bulky small molecule like a bile salt derivative, relatively rapid and fully complete, selective CM conversions were achieved, enabling preparation of these challenging structures in a few synthetic steps.

The improved hydrophilicity of each ASD polymer vs. the corresponding ethyl cellulose-bile salt adduct led to substantially increased nucleation-induction times (e.g., slower crystallization) even with the fast-crystallizing prostate cancer drug, enzulatamide. In some cases, bile salt adduct methyl esters performed better than the corresponding acids. This was a surprising result, given our earlier studies showing the value of carboxylic acid substituents in prolonging nucleation times. While carboxyl-containing polysaccharides have often performed well in crystallization inhibition (e.g., hydroxypropyl methyl cellulose acetate succinate is a leading commercial ASD polymer (Curatolo, Nightingale, & Herbig, 2009)) and in structure-property studies (Liu et al., 2014), it is also true that neutral cellulose ethers like HPC and hydroxypropyl methyl cellulose are effective ASD polymers for certain drugs (Arca, Mosquera-Giraldo, Pereira, et al., 2018), and neither contains carboxyl groups. This study highlights the importance of amphiphilic character of the polymer to ASD performance, indicating that, in this family of polymers at least, the absence of a pendent carboxylic acid to act as a pH trigger and provide amphiphilicity can be overcome by interactions between the hydrophobic bile salt methyl ester substituent and the drug. It also illustrates the complex nature of these structure property relationships, illustrated in Fig. S17 by comparing crystallization induction time of these polymers to solubility parameter, bile salt type and DS, and whether the terminus of the bile salt substituent was a carboxylic acid or a methyl ester. It is clear from the relationship that LCA derivatives performed better, as did those with higher DS (bile salt). While the methyl esterified LCA adduct gave the best performance, there was not a clear overall trend to better performance for the methyl esters. The best performers had solubility parameters between 21.5 and 22.5, but there were also several poor performers in that SP range.

In the best case, the methyl ester of LCA and pentenyl HPC adduct, in vitro enzalutamide crystallization time was nearly 8 h, considerably exceeding normal small intestine residence time. It was also gratifying and useful that the LCA derivatives performed best, since they are simpler to synthesize and pose less complex regioselectivity problems. It will be of great interest to probe further the structure property relationships of these cellulose ether–bile salt adducts, further illuminating features needed for truly superior crystallization inhibition even in difficult cases like enzalutamide, and providing further insight into the fundamental nature of and structural requirements for crystallization inhibition.

CRediT authorship contribution statement

Diana C. Novo: Investigation, Writing – original draft, Writing – review & editing, Conceptualization. **Chengzhe Gao:** Investigation. **Qingqing Qi:** Investigation. **Laura I. Mosquera-Giraldo:** Investigation, Writing – original draft. **Glenn A. Spiering:** Investigation. **Robert B. Moore:** Supervision, Conceptualization. **Lynne S. Taylor:** Conceptualization, Supervision, Writing – review & editing. **Kevin J. Edgar:** Conceptualization, Supervision, Writing – review & editing.

Declaration of competing interest

The authors declare that they have no known competing financial interests or personal relationships that could have appeared to influence the work reported in this paper.

Acknowledgements

This research was supported in part (DN) by the National Institutes of Health, through an Initiative to Maximize Student Development (award number R25GM072767) and the National Science Foundation (PFI-RP) for partial support of this work through grant IIP-1827493 (CG). We thank the Department of Chemistry at Virginia Tech and the Macromolecules and Innovations Institute for educational support, and the Institute for Critical Technology and Applied Science for facility support. We also thank Brady Hall of Virginia Tech for performing SEC experiments.

Appendix A. Supplementary data

Supplementary data to this article can be found online at https://doi.org/10.1016/j.carbpol.2022.119680.

References

Arca, H. C., Mosquera-Giraldo, L. I., Bi, V., Xu, D., Taylor, L. S., & Edgar, K. J. (2018). Pharmaceutical applications of cellulose ethers and cellulose ether esters. *Biomacromolecules, 19*(7), 2351–2376. https://doi.org/10.1021/acs.biomac.8b00517

Arca, H.Ç., Mosquera-Giraldo, L. I., Pereira, J. M., Sriranganathan, N., Taylor, L. S., & Edgar, K. J. (2018). Rifampin stability and solution concentration enhancement through amorphous solid dispersion in cellulose ω-carboxyalkanoate matrices. *Journal of Pharmaceutical Sciences, 107*(1), 127–138. https://doi.org/10.1016/J.XPHS.2017.05.036

Baird, J. A., Van Eerdenbrugh, B., & Taylor, L. S. (2010). A classification system to assess the crystallization tendency of organic molecules from undercooled melts. *Journal of Pharmaceutical Sciences, 99*(9), 3787–3806. https://doi.org/10.1002/JPS.22197

Fox, S. C., Li, B., Xu, D., & Edgar, K. J. (2011). Regioselective esterification and etherification of cellulose: A review. *Biomacromolecules, 12*(6), 1956–1972. https://doi.org/10.1021/bm200260d

Chatterjee, A. K., Choi, T.-L., Sanders, D. P., & Grubbs, R. H. (2003). A general model for selectivity in olefin cross metathesis. *Journal of the American Chemical Society, 125*(37), 11360–11370. https://doi.org/10.1021/ja0214882

Chen, J., Mosquera-Giraldo, L. I., Ormes, J. D., Higgins, J. D., & Taylor, L. S. (2015). Bile salts as crystallization inhibitors of supersaturated solutions of poorly water-soluble compounds. *Crystal Growth and Design, 15*(6), 2593–2597. https://doi.org/10.1021/acs.cgd.5b00392

Craig, D. Q. M. (2002). The mechanisms of drug release from solid dispersions in water-soluble polymers. *International Journal of Pharmaceutics, 231*(2), 131–144. https://doi.org/10.1016/S0378-5173(01)00891-2

Curatolo, W., Nightingale, J. A., & Herbig, S. M. (2009). Utility of hydroxypropylmethylcellulose acetate succinate (HPMCAS) for initiation and maintenance of drug supersaturation in the GI milieu. *Pharmaceutical Research, 26*(6), 1419–1431. https://doi.org/10.1007/s11095-009-9852-z

Dong, Y., & Edgar, K. J. (2015). Imparting functional variety to cellulose ethers via olefin cross-metathesis. *Polymer Chemistry, 6*(20), 3816–3827. https://doi.org/10.1039/C5PY00369E

Dong, Y., Matson, J. B., & Edgar, K. J. (2017). Olefin cross-metathesis in polymer and polysaccharide chemistry: A review. *Biomacromolecules, 18*(6), 1661–1676. https://doi.org/10.1021/acs.biomac.7b00364

Dong, Y., Mosquera-Giraldo, L. I., Taylor, L. S., & Edgar, K. J. (2016). Amphiphilic cellulose ethers designed for amorphous solid dispersion via olefin cross-metathesis. *Biomacromolecules, 17*(2), 454–465. https://doi.org/10.1021/acs.biomac.5b01336

Dong, Y., Mosquera-Giraldo, L. I., Taylor, L. S., & Edgar, K. J. (2017). Tandem modification of amphiphilic cellulose ethers for amorphous solid dispersion via olefin cross-metathesis and thiol-Michael addition. *Polymer Chemistry, 8*(20), 3129–3139. https://doi.org/10.1039/C7PY00228A

Dong, Y., Mosquera-Giraldo, L. I., Troutman, J., Skogstad, B., Taylor, L. S., & Edgar, K. J. (2016). Amphiphilic hydroxyalkyl cellulose derivatives for amorphous solid dispersion prepared by olefin cross-metathesis. *Polymer Chemistry, 7*(30), 4953–4963. https://doi.org/10.1039/C6PY00960C

Dong, Y., Novo, D. C., Mosquera-Giraldo, L. I., Taylor, L. S., & Edgar, K. J. (2019a). Conjugation of bile esters to cellulose by olefin cross-metathesis: A strategy for accessing complex polysaccharide structures. *Carbohydrate Polymers, 221*, 37–47. https://doi.org/10.1016/j.carbpol.2019.05.061

Dong, Y., Novo, D. C., Mosquera-Giraldo, L. I., Taylor, L. S., & Edgar, K. J. (2019b). Conjugation of bile esters to cellulose by olefin cross-metathesis: A strategy for accessing complex polysaccharide structures. *Carbohydrate Polymers, 221*, 37–47. https://doi.org/10.1016/J.CARBPOL.2019.05.061

Fedors, R. F. (1974). A method for estimating both the solubility parameters and molar volumes of liquids.Supplement. *Polymer Engineering & Science, 14*(6). https://doi.org/10.1002/pen.760140611, 472-472.

Fischer, E., & Speier, A. (1895). Darstellung der Ester. *Berichte der Deutschen Chemischen Gesellschaft, 28*(3), 3252–3258. https://doi.org/10.1002/CBER.189502803176

Frank, D. S., & Matzger, A. J. (2018). Probing the interplay between amorphous solid dispersion stability and polymer functionality. *Molecular Pharmaceutics, 15*(7), 2714–2720. https://doi.org/10.1021/acs.molpharmaceut.8b00219

Ricarte, R. G., Van Zee, N. J., Li, Z., Johnson, L. M., Lodge, T. P., & Hillmyer, M. A. (2019). Recent advances in understanding the micro- and nanoscale phenomena of amorphous solid dispersions. *Molecular Pharmaceutics, 16*(10), 4089–4103. https://doi.org/10.1021/acs.molpharmaceut.9b00601

Grubbs, R. H. (2004). Olefin metathesis. *Tetrahedron, 60*(34), 7117–7140. https://doi.org/10.1016/j.tet.2004.05.124

Hasegawa, A., Taguchi, M., Suzuki, R. I. E., Miyata, T., Nakagawa, H., & Sugimoto, I. (1988). Supersaturation mechanism of drugs from solid dispersions with enteric coating agents. *Chemical & Pharmaceutical Bulletin, 36*(12), 4941–4950. https://doi.org/10.1248/cpb.36.4941

Hu, X., Zhang, Z., Zhang, X., Li, Z., & Zhu, X. X. (2005). Selective acylation of cholic acid derivatives with multiple methacrylate groups. *Steroids, 70*(8), 531–537. https://doi.org/10.1016/j.steroids.2004.11.015

Ilevbare, G. A., Liu, H., Edgar, K. J., & Taylor, L. S. (2013a). Maintaining supersaturation in aqueous drug solutions: Impact of different polymers on induction times. *Crystal Growth & Design, 13*(2), 740–751. https://doi.org/10.1021/cg301447d

Ilevbare, G. A., Liu, H., Edgar, K. J., & Taylor, L. S. (2013b). Impact of polymers on crystal growth rate of structurally diverse compounds from aqueous solution. *Molecular Pharmaceutics, 10*(6), 2381–2393. https://doi.org/10.1021/mp400029v

Jackson, M. J., Kestur, U. S., Hussain, M. A., & Taylor, L. S. (2016). Dissolution of danazol amorphous solid dispersions: Supersaturation and phase behavior as a function of drug loading and polymer type. *Molecular Pharmaceutics, 13*(1), 223–231. https://doi.org/10.1021/ACS.MOLPHARMACEUT.5B00652/ASSET/IMAGES/ACS.MOLPHARMACEUT.5B00652.SOCIAL.JPEG_V03

Li, N., Mosquera-Giraldo, L. I., Borca, C. H., Ormes, J. D., Lowinger, M., Higgins, J. D., Slipchenko, L. V., & Taylor, L. S. (2016). A comparison of the crystallization inhibition properties of bile salts. *Crystal Growth & Design, 16*(12), 7286–7300. https://doi.org/10.1021/acs.cgd.6b01470

Li, Y., & Ray Dias, J. (1997). Dimeric and oligomeric steroids. *Chemical Reviews, 97*(1), 283–304. https://doi.org/10.1021/cr9600565

Liu, H., Ilevbare, G. A., Cherniawski, B. P., Ritchie, E. T., Taylor, L. S., & Edgar, K. J. (2014). Synthesis and structure-property evaluation of cellulose ω-carboxyesters for amorphous solid dispersions. *Carbohydrate Polymers, 100*, 116–125. https://doi.org/10.1016/j.carbpol.2012.11.049

Liu, H., Taylor, L. S., & Edgar, K. J. (2015). The role of polymers in oral bioavailability enhancement; a review. *Polymer, 77*, 399–415. https://doi.org/10.1016/J.POLYMER.2015.09.026

Lu, J., Ormes, J. D., Lowinger, M., Mann, A. K. P., Xu, W., Litster, J. D., & Taylor, L. S. (2017). Maintaining supersaturation of active pharmaceutical ingredient solutions with biologically relevant bile salts. *Crystal Growth & Design, 17*(5), 2782–2791. https://doi.org/10.1021/acs.cgd.7b00237

Lu, J., Ormes, J. D., Lowinger, M., Mann, A. K. P., Xu, W., Patel, S., Litster, J. D., & Taylor, L. S. (2017). Impact of bile salts on solution crystal growth rate and residual supersaturation of an active pharmaceutical ingredient. *Crystal Growth & Design, 17*(6), 3528–3537. https://doi.org/10.1021/acs.cgd.7b00464

Meng, X., & Edgar, K. J. (2015). Synthesis of amide-functionalized cellulose esters by olefin cross-metathesis. *Carbohydrate Polymers, 132*, 565–573. https://doi.org/10.1016/j.carbpol.2015.06.052

Meng, X., Matson, J. B., & Edgar, K. J. (2014). Olefin cross-metathesis, a mild, modular approach to functionalized cellulose esters. *Polymer Chemistry, 5*(24), 7021–7033. https://doi.org/10.1039/C4PY01102C

Mosquera-Giraldo, L. I., Borca, C. H., Meng, X., Edgar, K. J., Slipchenko, L. V., & Taylor, L. S. (2016). Mechanistic design of chemically diverse polymers with applications in oral drug delivery. *Biomacromolecules, 17*(11), 3659–3671. https://doi.org/10.1021/acs.biomac.6b01156

Mosquera-Giraldo, L. I., Borca, C. H., Parker, A. S., Dong, Y., Edgar, K. J., Beaudoin, S. P., … Taylor, L. S. (2018). Crystallization inhibition properties of cellulose esters and ethers for a group of chemically diverse drugs: Experimental and computational insight. *Biomacromolecules, 19*(12), 4593–4606. https://doi.org/10.1021/acs.biomac.8b01280

Mosquera-Giraldo, L. I., Li, N., Wilson, V. R., Nichols, B. L. B., Edgar, K. J., & Taylor, L. S. (2018). Influence of polymer and drug loading on the release profile and membrane transport of telaprevir. *Molecular Pharmaceutics, 15*(4), 1700–1713. https://doi.org/10.1021/acs.molpharmaceut.8b00104

Mukhopadhyay, S., & Maitra, U. (2004). Chemistry and biology of bile acids. *Current Science, 87*(12), 1666–1683. http://www.jstor.org/stable/24109764 http://www.jstor.org/stable/24109764.

Pavlović, N., Goločorbin-Kon, S., Danić, M., Stanimirov, B., Al-Salami, H., Stankov, K., & Mikov, M. (2018). Bile acids and their derivatives as potential modifiers of drug release and pharmacokinetic profiles. *Frontiers in Pharmacology, 9*(NOV). https://doi.org/10.3389/FPHAR.2018.01283/FPHAR_09_01283_PDF.PDF

Pereira, J. M., Mejia-Ariza, R., Ilevbare, G. A., McGettigan, H. E., Sriranganathan, N., Taylor, L. S., Davis, R. M., & Edgar, K. J. (2013). Interplay of degradation, dissolution and stabilization of clarithromycin and its amorphous solid dispersions. *Molecular Pharmaceutics, 10*(12), 4640–4653. https://doi.org/10.1021/MP400441D/SUPPL_FILE/MP400441D_SI_001.PDF

Sanford, M. S., Love, J. A., & Grubbs, R. H. (2001). Mechanism and activity of ruthenium olefin metathesis catalysts. *Journal of the American Chemical Society, 123*(27), 6543–6554. https://doi.org/10.1021/ja010624k

Tanno, F., Nishiyama, Y., Kokubo, H., & Obara, S. (2004). Evaluation of hypromellose acetate succinate (HPMCAS) as a carrier in solid dispersions. *Drug Development and Industrial Pharmacy, 30*(1), 9–17. https://doi.org/10.1081/DDC-120027506

Taylor, L. S., & Zhang, G. G. Z. (2016). Physical chemistry of supersaturated solutions and implications for oral absorption. *Advanced Drug Delivery Reviews, 101*, 122–142. https://doi.org/10.1016/J.ADDR.2016.03.006

Trasi, N. S., & Taylor, L. S. (2015). Dissolution performance of binary amorphous drug combinations—Impact of a second drug on the maximum achievable supersaturation. *International Journal of Pharmaceutics, 496*(2), 282–290. https://doi.org/10.1016/J.IJPHARM.2015.10.026

Van Eerdenbrugh, B., Baird, J. A., & Taylor, L. S. (2010). Crystallization tendency of active pharmaceutical ingredients following rapid solvent evaporation—Classification and comparison with crystallization tendency from under cooled melts. *Journal of Pharmaceutical Sciences, 99*(9), 3826–3838. https://doi.org/10.1002/JPS.22214

Van Eerdenbrugh, B., Raina, S., Hsieh, Y. L., Augustijns, P., & Taylor, L. S. (2014). Classification of the crystallization behavior of amorphous active pharmaceutical ingredients in aqueous environments. *Pharmaceutical Research, 31*(4), 969–982. https://doi.org/10.1007/S11095-013-1216-Z/TABLES/5

Wilson, V., Lou, X., Osterling, D. J., Stolarik, D. F., Jenkins, G., Gao, W., Zhang, G. G. Z., & Taylor, L. S. (2018). Relationship between amorphous solid dispersion in vivo absorption and in vitro dissolution: Phase behavior during dissolution, speciation, and membrane mass transport. *Journal of Controlled Release: Official Journal of the Controlled Release Society, 292*, 172–182. https://doi.org/10.1016/j.jconrel.2018.11.003

Wilson, V. R., Lou, X., Osterling, D. J., Stolarik, D. F., Jenkins, G. J., Nichols, B. L. B., Dong, Y., Edgar, K. J., Zhang, G. G. Z., & Taylor, L. S. (2020). Amorphous solid dispersions of enzalutamide and novel polysaccharide derivatives: Investigation of relationships between polymer structure and performance. *Scientific Reports, 10*(1), 18535. https://doi.org/10.1038/s41598-020-75077-7

Zhu, X.-X., & Nichifor, M. (2002). Polymeric materials containing bile acids. *Accounts of Chemical Research, 35*(7), 539–546. https://doi.org/10.1021/ar0101180